IEEE Access
Multidisciplinary | Rapid Review | Open Access Journal

Received March 29, 2020, accepted April 7, 2020, date of publication April 10, 2020, date of current version May 8, 2020.

Digital Object Identifier 10.1109/ACCESS.2020.2987277

Generalized State Space Average Model for Multi-Phase Interleaved Buck, Boost and Buck-Boost DC-DC Converters: Transient, Steady-State and Switching Dynamics

PETER AZER, (Graduate Student Member, IEEE), AND ALI EMADI, (Fellow, IEEE)
McMaster Institute for Automotive Research and Technology, McMaster University, Hamilton, ON L8P 0A6, Canada

Corresponding author: Peter Azer (eliap@mcmaster.ca)

This work was supported by the Canada Excellence Research Chairs (CERC) Program, and in part by the Natural Sciences and Engineering Research Council of Canada (NSERC).

ABSTRACT This paper presents a generalized state space average model (GSSAM) for multi-phase interleaved buck, boost and buck-boost converters. The GSSAM can model the switching behavior of the current and voltage waveforms, unlike the conventional average model which can model only the average value. The GSSAM is used for the converters with dominant oscillatory behavior such as resonant converters, high current ripple converters, and multi-converter systems. The maximum current and voltage through the system can be predicted by modeling the switching behavior of voltage and current. The GSSAM in the literature is introduced for single-phase converters only, and it is not introduced for multi-phase converters due to the high complexity associated with it. Hence, the GSSAM for multi-phase buck, boost and buck-boost converters are introduced in this paper and the proposed models can fit with converters of any number of phases. The number of operating phases in the multi-phase interleaved converters is proportional with the output power to achieve the maximum efficiency over the operating range. Therefore, the proposed GSSAMs can describe the operation at any number of operating phases with switching dynamics of phases. The proposed GSSAM is validated by comparing the transient and steady-state dynamics between the GSSAM and a switching model from PLECS.

INDEX TERMS Interleaved multi-phase dc-dc Converters, generalized state space average model, buck converter, boost converter, buck-boost converter.

I. INTRODUCTION

DC-DC converters are widely used in power system applications, aircraft power system, More Electric Aircraft (MEA), hybrid and electric vehicles [1]–[4]. Switching model of DC-DC converters cannot be used to simulate converter dynamics for large time periods like drive cycles which can exceed 2000 seconds, as it requires long simulation time and high processing units. Thus, the state space average model is used to model power converters for long-time simulations and in designing the control system [5], [7].

The conventional state space average model deals with the system as a small signal model which enables the linearization of state variables and cannot represent large signal dynamics. At large signal model, the magnitude of the AC signals can not be neglected, in other words, the Fourier representation of system dynamics includes not only the zero-order harmonic as a dominant value but also higher order harmonics.

DC-DC converters usually can be represented as a small signal model since the zero-order is the most dominant and effective value, except in the cases which have a dominant oscillatory behavior such as resonant converters, high current ripples converters, and multi-converter system [8], [9]. In these cases, a large signal model with time-dependent coefficients to describe the AC signals is used. This is referred by the generalized state space average model (GSSAM) which is created to describe the converter state variables by Fourier series including the zero and the first order harmonics approximation. GSSAM is introduced for single-phase buck,

The associate editor coordinating the review of this manuscript and approving it for publication was Zhehan Yi.

boost and buck-boost converters in [9] and [10], then it is extended for a multi-converter system including several DC-DC converters and single-phase voltage source inverter (VSI) in [8]. The multi-converter system in [8] in extended to include an interconnected buck converter with LC filter to decrease current ripples for more electric ship power system in [11].

Regarding other converters rather than DC-DC converters, GSSAM is also used to describe the oscillatory behavior of series resonant converters with voltage source load or a capacitor load in [12], and for parallel resonant converters in [13]. GSSAM of active filters like single-phase series and shunt active filters for control and stability aspects is introduced in [14]. GSSAM is used for 2-level and multi-level inverters [15]–[18].

Since the GSSAM can describe the switching behavior, therefore, it can replace the switching model. Additionally, the GSSAM runs around 1000 times faster than the switching model [6], [7]. Hence, the GSSAM can be used to represent the multi-phase converters for long drive cycle simulations including electro-thermal modeling. The conventional average model can be used for that purpose as well where switching oscillations are ignored [6], [7]. However, for converters with dominant oscillatory behavior, the conventional average model is not accurate, and the oscillatory behavior cannot be ignored in both the electrical and thermal simulations. The GSSAM is also used in designing the control schemes of converters and in estimating voltage and current overshoots for different control systems, for instance, the control schemes of single-phase full bridge rectifiers based on GSSAM are introduced in [19] and [20]. The DC voltage ripple is an important concern in DC grids, the GSSAM can be used for this purpose as it can describe voltage ripples [21], [22], unlike the conventional average model which cannot describe the switching dynamics of converters. System level modeling of multiconverters requires high processing units and long simulation time. Hence, the GSSAM can be used to increase the simulation time step and to reduce the simulation running time and system complexity [11]. The GSSAM can also predict converter performance during the design stage [3] as it is about 1000 times faster than the switching models. To sum up, the GSSAM is a dynamic model that can represent converter steady-state and transient dynamics similar to the switching model, but the GSSAM is much faster than the switching model.

Single-phase DC-DC converters have the maximum efficiency at the rated load conditions and it has low efficiency operation at partially loaded conditions. Thus, the multi-phase interleaved DC-DC converters are introduced to achieve high efficiency among the entire loading range so that the number of operating phases is proportional to the output load power [21]. GSSAM for multi-phase DC-DC converters is not proposed before in literature due to the complexity of the high number of state variables. In this paper, GSSAM for multi-phase interleaved buck, boost and buck-boost DC-DC converters is introduced. The proposed GSSAM can be used for any number of phases. Since the number of the operating phases in interleaved converters is proportional with the load, the proposed GSSAM can present the operation at any number of active phases. Furthermore, the proposed model can describe the switching dynamics of phases. The GSSAM is validated by comparing the steady-state and transient dynamics between the GSSAM and PLECS switching model of buck, boost and buck-boost converters. The factors that affect the error between the GSSAM and the switching model are investigated, and the essential parameters required to describe switching dynamics of phases are discussed in detail.

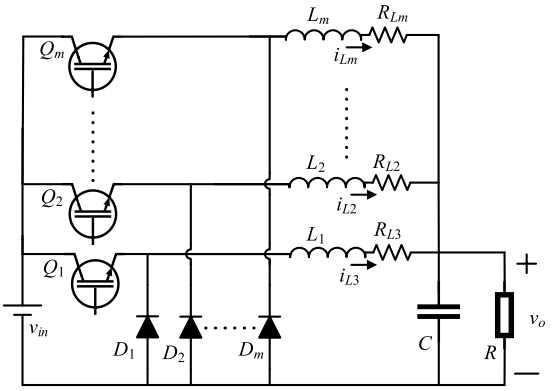

FIGURE 1. Multi-phase DC-DC buck converter.

The paper is organized as follows, Section II presents the GSSAMs of multi-phase buck, boost and buck-boost converters. Section III validates the proposed GSSAM using 3-phase buck, boost and buck-boost converters. Section IV presents the conclusion of the paper.

II. ANALYSIS OF MULTI-PHASE DC-DC CONVERTERS

A. BUCK CONVERTER

Multi-phase buck converter is shown in Fig. 1, the differential equations describing the buck converter are:

$$\sum_{i=1}^{m} \frac{di_{Li}}{dt} = \frac{1}{L_i}\left(V_{in}.u_i\left(t\right) - v_o - i_{Li}R_{Li}\right) \tag{1}$$

$$\sum_{i=1}^{m} \frac{dv_o}{dt} = \frac{1}{c}\left(i_{Li} - \frac{v_o}{R}\right) \tag{2}$$

where i_{Li} is the phase current (or the inductor current) and m is the number of phases, V_{in} is the input DC voltage and v_o is the output voltage. R_{Li} is the inductor parasitic resistance. c is the output capacitance and R is the load resistance. $u_i(t)$ is the control signal of the controlled switch 'Q' and is equal to one and zero at switching on and off, respectively. Thus, $u_i(t)$ is represented as:

$$u_i\left(t\right) = \begin{Bmatrix} 1, & 0 < t < T_{on} \\ 0, & T_{on} < t < T_{off} \end{Bmatrix}, \quad T_{on} = D_i T \tag{3}$$

where D_i is the duty cycle of the switch. T is the switching period. T_{on} and T_{off} and the turn-on and turn-off switching times. The state variables can be expressed by Fourier series

as:

$$f(x) = \frac{a_o}{2} + \sum_{n=1}^{\infty} (a_n \cos(nx) + b_n \sin(nx)) \tag{4}$$

where a_o is the DC component. a_n and b_n are the cosine and sine Fourier coefficient, respectively. Converting the trigonometric functions into Euler's formula:

$$\cos(nx) = \frac{e^{jnx} + e^{-jnx}}{2}, \quad \sin(nx) = \frac{e^{jnx} - e^{-jnx}}{2j} \tag{5}$$

Substituting (5) in (4):

$$\begin{aligned} f(x) &= \frac{a_o}{2} + \sum_{n=1}^{\infty} e^{jnx}\left(\frac{a_n - jb_n}{2}\right) + \sum_{n=1}^{\infty} e^{-jnx}\left(\frac{a_n + jb_n}{2}\right) \\ &= \sum_{n=-\infty}^{\infty} c_n e^{jnx} \end{aligned} \tag{6}$$

where c_n and c_{-n} are complex and conjugate to each other. Converting (6) into time domain, where the fundamental frequency is the switching frequency:

$$f(t) = \sum_{n=-\infty}^{\infty} c_n e^{jnw_s t}, \quad w_s = 2\pi f_{sw} \tag{7}$$

By considering zero and first order approximation:

$$f(t) = c_0 + c_{-1}e^{-jw_s t} + c_{+1}e^{+jw_s t} \tag{8}$$

Thus, the buck converter state variables are the inductor currents and capacitor voltage, and they are represented as:

$$i_{Li} = i_{Li,0} + i_{Li,-1}e^{-jw_s t} + i_{Li,+1}e^{+jw_s t} \tag{9a}$$
$$i_{Li,+1} = x_{2i-1} + jx_{2i} \tag{9b}$$
$$i_{Li,-1} = x_{2i-1} - jx_{2i} \tag{9c}$$
$$i_{Li,0} = x_{2(m+1)+i} \tag{9d}$$

where x_{2i-1} and x_{2i} are the state variables of the first order harmonic of inductor phase current i_{Li}, and $x_{2(m+1)+i}$ is the state variable of the zero order harmonic of i_{Li}.

$$v_o = v_{oi,0} + v_{oi,-1}e^{-jw_s t} + v_{oi,+1}e^{+jw_s t} \tag{10a}$$
$$v_{o,+1} = x_{2m+1} + jx_{2m+2} \tag{10b}$$
$$v_{o,-1} = x_{2m+1} - jx_{2m+2} \tag{10c}$$
$$v_{o,0} = x_{3(m+1)} \tag{10d}$$

where x_{2m+1} and x_{2m+2} are the state variables of the first order harmonic of capacitor voltage v_o, and $x_{3(m+1)}$ is the state variable of the zero order harmonic of v_o. The order of the state variables in (9) and (10) is selected so that the final state space matrix is arranged to have the first order state variables of inductor currents i_{Li}, then the first order state variables of the capacitor voltage v_o, following by the zero order state variable of i_{Li} and finally the zero order state variable of the v_o.

The control signal $u_i(t)$ is represented by Fourier transform. Since the control signal defined in (1) has constant values over time intervals $[0, D_iT]$ and $[D_iT, T]$, therefore, the coefficients of the control signal $u_i(t)$ are dependent on duty cycle and independent of time. The calculation of the zero and first order harmonics of the control signal is calculated by Fourier transform as the control signal is a known input, unlike the state variables which are unknown outputs in the system:

$$U(f_n) = \frac{1}{T}\int_{-\frac{T}{2}}^{\frac{T}{2}} u(t)e^{-jnw_s t}dt = \frac{1}{T}\int_{0}^{T} u(t)e^{-jnw_s t}dt \tag{11}$$
$$u_i(t) = U_i(f_0) + U_i(f_1) \tag{12}$$
$$U_i(f_0) = \frac{1}{T}\int_{0}^{D_iT} 1\,dt = D_i \tag{13}$$
$$\begin{aligned} U_i(f_1) &= \frac{1}{T}\int_{0}^{D_iT} e^{-jw_s t}dt = \frac{1}{T}\left[\frac{e^{-jw_s t}}{-jw_s}\right]_0^{D_iT} \\ &= \frac{j}{T}\left[\frac{e^{-\frac{j2\pi t}{T}}}{\frac{2\pi}{T}}\right]_0^{D_iT} = \frac{j}{2\pi}\left[e^{-j2\pi D_i} - 1\right] \\ &= -\frac{\sin(2\pi D_i)}{2\pi} - j\frac{[\sin(\pi D_i)]^2}{\pi} \end{aligned} \tag{14}$$
$$u_i(t) = D_i - \frac{\sin(2\pi D_i)}{2\pi} - j\frac{[\sin(\pi D_i)]^2}{\pi} \tag{15}$$

Writing (9) in the trigonometric form:

$$\begin{aligned} i_{Li} &= x_{2(m+1)+i} + (x_{2i-1} - jx_{2i})\,e^{-jw_s t} + (x_{2i-1} + jx_{2i})\,e^{+jw_s t} \\ &= x_{2(m+1)+i} + x_{2i-1}\begin{pmatrix} \cos(-w_s t) + j\sin(-w_s t) \\ +\cos(w_s t) + j\sin(w_s t) \end{pmatrix} \\ &\quad + jx_{2i}\begin{pmatrix} \cos(w_s t) + j\sin(w_s t) \\ +\cos(-w_s t) + j\sin(-w_s t) \end{pmatrix} \\ &= x_{2(m+1)+i} + 2x_{2i-1}\cos(w_s t) - 2x_{2i}\sin(w_s t) \end{aligned} \tag{16}$$

similarly, for v_o in (10):

$$v_o = x_{3(m+1)} + 2x_{2m+1}\cos(w_s t) - 2x_{2m+2}\sin(w_s t) \tag{17}$$

The derivatives of state variables in (16) and (17) are:

$$\begin{aligned} i_{Li}^o &= x_{2(m+1)+i}^o + 2x_{2i-1}^o\cos(w_s t) - 2x_{2i-1}w_s\sin(w_s t) \\ &\quad - 2x_{2i}^o\sin(w_s t) - 2x_{2i}w_s\cos(w_s t) \end{aligned} \tag{18}$$
$$\begin{aligned} v_o^o &= x_{3(m+1)}^o + 2x_{2m+1}^o\cos(w_s t) - 2x_{2m+1}w_s\sin(w_s t) \\ &\quad - 2x_{2m+2}^o\sin(w_s t) - 2x_{2m+2}w_s\cos(w_s t) \end{aligned} \tag{19}$$

By substituting (15), (16), (17) and (18) in (1), and (16), (17) and (19) in (2), and comparing the coefficients of $\cos(w_s t)$, $\sin(w_s t)$ and the DC values, the GSSAM of the m-phase buck converter is obtained (20), as shown at the bottom of the next page. The GSSAM in (20) is divided into several inner

matrices which depend on the number of phases, m of the buck converter. The exact location of these inner matrices is defined by the row and column numbers which are function of the number of phases, m.

B. BOOST CONVERTER

Fig. 2 shows an m-phase boost converter, and it can be described as:

$$\sum_{i=1}^{m} \frac{di_{Li}}{dt} = \frac{1}{L_i}\left(V_{in} - (1 - u_i(t))\, v_o - i_{Li} R_{Li}\right) \quad (21)$$

$$\sum_{i=1}^{m} \frac{dv_o}{dt} = \frac{1}{c}\left[i_{Li}(1 - u_i(t)) - \frac{v_o}{R}\right] \quad (22)$$

State variables of inductor currents and capacitor voltage of boost converter is similar to buck converters in (9)-(19).

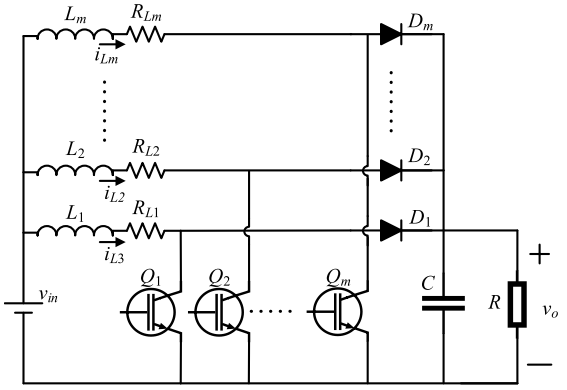

FIGURE 2. Multi-phase DC-DC boost converter.

Substituting (9)-(19) in (21) and (22), the GSSAM of the m-phase boost converter is presented in (23), as shown at the top of the next page.

$$\begin{bmatrix} x_1^{o} \\ \vdots \\ x_{2m}^{o} \\ x_{2m+1}^{o} \\ x_{2m+2}^{o} \\ x_{2m+3}^{o} \\ \vdots \\ x_{3m+2}^{o} \\ x_{3(m+1)}^{o} \end{bmatrix}_{3(m+1)\times 1} = \begin{bmatrix} (\sin(2\pi D_1))/2\pi L_1 \\ -(\sin(\pi D_1))^2/\pi L_1 \\ \vdots \\ (\sin(2\pi D_m))/2\pi L_m \\ -(\sin(\pi D_m))^2/\pi L_m \\ 0 \\ 0 \\ D_1/L_1 \\ \vdots \\ D_m/L_m \\ 0 \end{bmatrix}_{3(m+1)\times 1} V_{in} + A_1 \begin{bmatrix} x_1 \\ \vdots \\ x_{2m} \\ x_{2m+1} \\ x_{2m+2} \\ x_{2m+3} \\ \vdots \\ x_{3m+2} \\ x_{3(m+1)} \end{bmatrix}_{3(m+1)\times 1} \quad (20)$$

$$A_1 = \begin{bmatrix} -R_{L1}/L_1 & W & 0 & 0 & 0 & 0 & -1/L_1 & 0 & 0 & 0 & 0 & 0 \\ -W & -R_{L1}/L_1 & 0 & 0 & 0 & 0 & 0 & -1/L_1 & 0 & 0 & 0 & 0 \\ 0 & 0 & \ddots & & 0 & 0 & \vdots & & 0 & 0 & 0 & 0 \\ 0 & 0 & & \ddots & 0 & 0 & & & 0 & 0 & 0 & 0 \\ 0 & 0 & 0 & 0 & -R_{Lm}/L_m & W & -1/L_m & 0 & 0 & 0 & 0 & 0 \\ 0 & 0 & 0 & 0 & -W & -R_{Lm}/L_m & 0 & -1/L_m & 0 & 0 & 0 & 0 \\ 1/C & 0 & \cdots & & 1/C & 0 & -1/RC & W & 0 & 0 & 0 & 0 \\ 0 & 1/C & & & 0 & 1/C & -W & -1/RC & 0 & 0 & 0 & 0 \\ 0 & 0 & 0 & 0 & 0 & 0 & 0 & 0 & -R_{L1}/L_1 & 0 & 0 & -1/L_1 \\ 0 & 0 & 0 & 0 & 0 & 0 & 0 & 0 & 0 & \ddots & 0 & \vdots \\ 0 & 0 & 0 & 0 & 0 & 0 & 0 & 0 & 0 & 0 & -R_{Lm}/L_m & -1/L_m \\ 0 & 0 & 0 & 0 & 0 & 0 & 0 & 0 & 1/C & \cdots & 1/C & -1/RC \end{bmatrix}_{3(m+1)\times 3(m+1)}$$

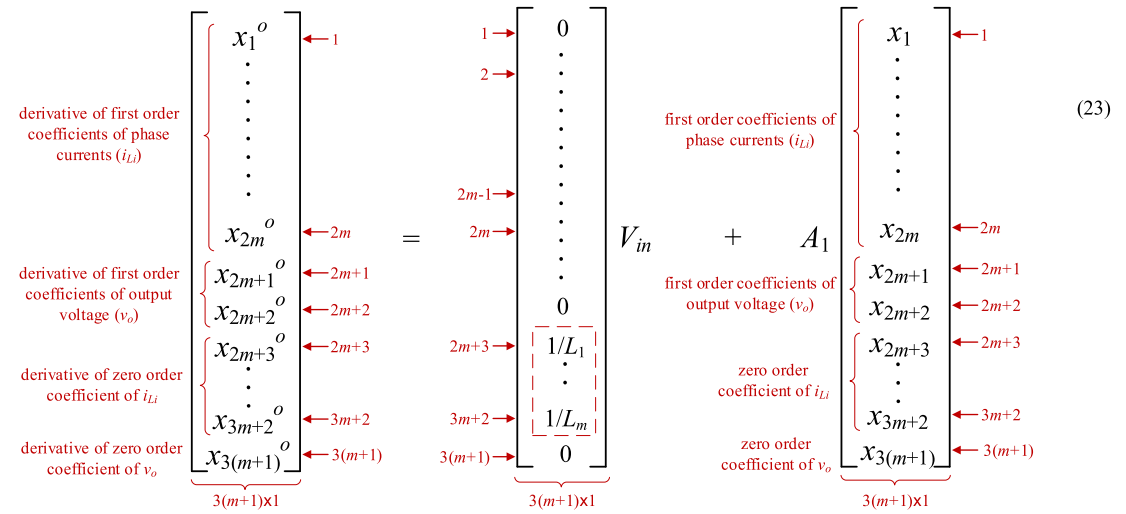

(23)

$$A_1=\begin{bmatrix}
-R_{L1}/L_1 & W & 0 & 0 & 0 & 0 \\
-W & -R_{L1}/L_1 & 0 & 0 & 0 & 0 \\
0 & 0 & \ddots & & 0 & 0 \\
0 & 0 & & \ddots & 0 & 0 \\
0 & 0 & 0 & 0 & -R_{Lm}/L_m & W \\
0 & 0 & 0 & 0 & -W & -R_{Lm}/L_m \\
(1-D_1)/C & 0 & \cdots & & (1-D_m)/C & 0 \\
0 & (1-D_1)/C & & & 0 & (1-D_m)/C \\
0 & 0 & 0 & 0 & 0 & 0 \\
0 & 0 & 0 & 0 & 0 & 0 \\
0 & 0 & 0 & 0 & 0 & 0 \\
-(\sin(2\pi D_1))/\pi C & 2(\sin(\pi D_1))^2/\pi C & \cdots & & -(\sin(2\pi D_m))/\pi C & 2(\sin(\pi D_m))^2/\pi C
\end{bmatrix}$$

$3(m+1)\times 3(m+1)$

$$\begin{bmatrix}
-(1-D_1)/L_1 & 0 & 0 & 0 & 0 & (\sin(2\pi D_1))/2\pi L_1 \\
0 & -(1-D_1)/L_1 & 0 & 0 & 0 & -(\sin(\pi D_1))^2/2\pi L_1 \\
 & & 0 & 0 & 0 & \\
 & & 0 & 0 & 0 & \\
-(1-D_m)/L_m & 0 & 0 & 0 & 0 & (\sin(2\pi D_m))/2\pi L_m \\
0 & -(1-D_m)/L_m & 0 & 0 & 0 & -(\sin(\pi D_m))^2/2\pi L_m \\
-1/RC & W & -(\sin(2\pi D_1))/2\pi C & \cdots & -(\sin(2\pi D_m))/2\pi C & 0 \\
-W & -1/RC & (\sin(\pi D_1))^2/\pi C & & (\sin(\pi D_m))^2/\pi C & 0 \\
(\sin(2\pi D_1))/\pi L_1 & -2(\sin(\pi D_1))^2/\pi L_1 & -R_{L1}/L_1 & 0 & 0 & -(1-D_1)/L_1 \\
 & & 0 & \ddots & 0 & \\
(\sin(2\pi D_m))/\pi L_m & -2(\sin(\pi D_m))^2/\pi L_m & 0 & 0 & -R_{Lm}/L_m & -(1-D_m)/L_m \\
0 & 0 & (1-D_1)/C & \cdots & (1-D_m)/C & -1/RC
\end{bmatrix}$$

TABLE 1. Converter parameters.

Converter	V_{in} (V)	L (uH)	R_L (Ω)	C (uF)	R (Ω)	F_{sw} (kHz)
Boost	140	21.2	0.1	160	5	75
Buck and Buck-Boost	60	1	0.002	10	10	10

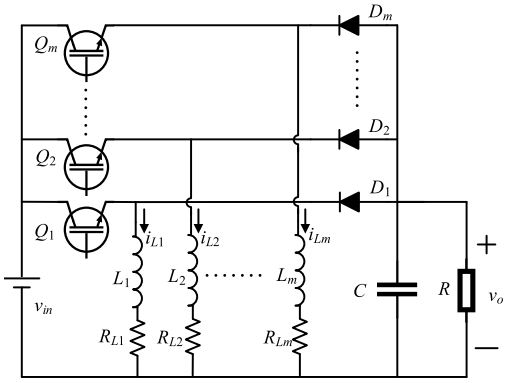

FIGURE 3. Multi-phase DC-DC buck-boost converter.

C. BUCK-BOOST CONVERTER

The differential equations describing the m-phase buck-boost converter, which is shown in Fig. 3, are:

$$\sum_{i=1}^{m} \frac{di_{Li}}{dt} = \frac{1}{L_i}\left(V_{in}u_i(t) - (1-u_i(t))\,v_o - i_{Li}.R_{Li}\right) \quad (24)$$

$$\sum_{i=1}^{m} \frac{dv_o}{dt} = \frac{1}{c}\left[i_{Li}(1-u_i(t)) - \frac{v_o}{R}\right] \quad (25)$$

Substituting (9)-(19) in (24) and (25), the GSSAM of the m-phase buck-boost converter is presented in (26), as shown at the top of the next page. It is worth mentioning that the derivation of GSSAM is more complex compared to the switching models. However, the implementation of the GSSAM is the same complex level as the switching models, since the complexity of the GSSAM is the derivation of the final matrix and once the final matrix is obtained (equations (20), (23), (26)), the implementation of the GSSAM is not a complicated process.

III. RESULTS AND DISCUSSION

The GSSAM for a 3-phase converters, buck, boost and buck-boost is used for validation by comparing it with a PLECS switching model at different duty cycles. Table. 1 shows the parameters of the converters which are used in investigation.

A. ERROR DEPENDENCY

Figs. 4-6 compare the system dynamics between the GSSAM and the switching model for buck, boost and buck-boost converters, respectively. Simulation results show that the error between the proposed GSSAM and the switching model depends on duty cycle and converter topology (buck or boost or buck-boost). These parameters are presented in the next section.

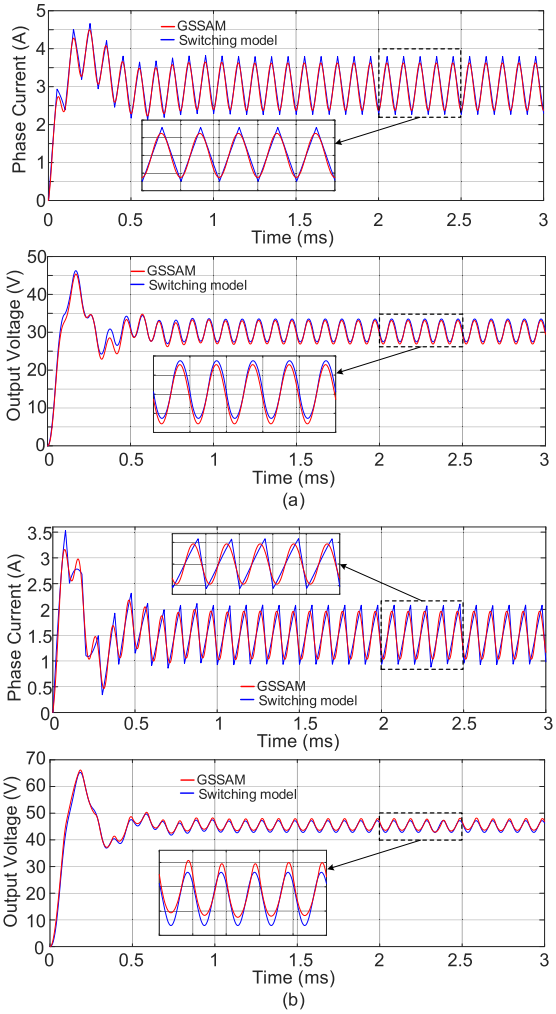

FIGURE 4. Buck converter dynamics from the switching model and GSSAM at duty cycle equals to (a) 0.5. (b) 0.75.

1) DUTY CYCLE

As mentioned in the previous section, the GSSAM considers only the zero and first order harmonics, while the switching model contains infinite number of harmonics which in return ends up by the sharp saw-tooth current waveform. When the duty cycle is equal to 0.5, the switching model contains odd order harmonics only, thus, error between the GSSAM and the switching model is the minimum as shown in simulation results.

2) CONVERTER COMPLEXITY

It can be concluded from Fig. 4 that the buck converter has the minimum error when duty cycle is equal to 0.75 compared to the boost and the buck-boost converters at the same duty cycle in Fig. 5 and Fig. 6. This is due to topology complexity, since in buck converter the controlled signal $u(t)$ is multiplied by the input signal V_{in}, while in the case of boost and buck-boost converters, the controlled signal is multiplied by the state variables which are approximated in the GSSAM by considering the zero and first order harmonics only. Therefore,

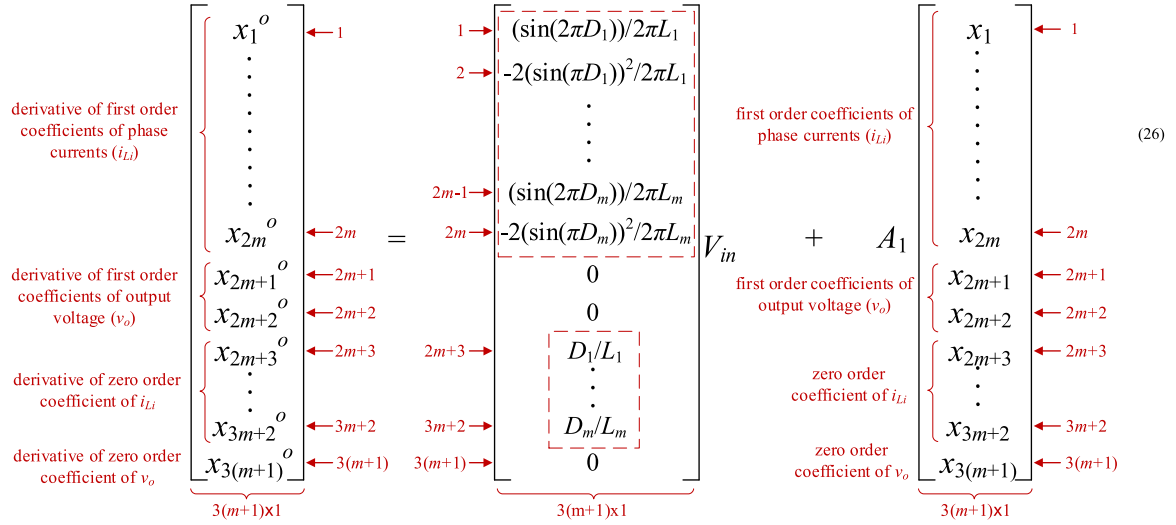
derivative of first order coefficients of phase currents (i_{Li})
derivative of first order coefficients of output voltage (v_o)
derivative of zero order coefficient of i_{Li}
derivative of zero order coefficient of v_o
x_1^o
x_{2m}^o
x_{2m+1}^o
x_{2m+2}^o
x_{2m+3}^o
x_{3m+2}^o
$x_{3(m+1)}^o$
$3(m+1)$x1
$(\sin(2\pi D_1))/2\pi L_1$
$-2(\sin(\pi D_1))^2/2\pi L_1$
$(\sin(2\pi D_m))/2\pi L_m$
$-2(\sin(\pi D_m))^2/2\pi L_m$
0
D_1/L_1
D_m/L_m
V_{in}
+
A_1
first order coefficients of phase currents (i_{Li})
first order coefficients of output voltage (v_o)
zero order coefficient of i_{Li}
zero order coefficient of v_o
x_1
x_{2m}
x_{2m+1}
x_{2m+2}
x_{2m+3}
x_{3m+2}
$x_{3(m+1)}$

(26)

$$A_1=$$

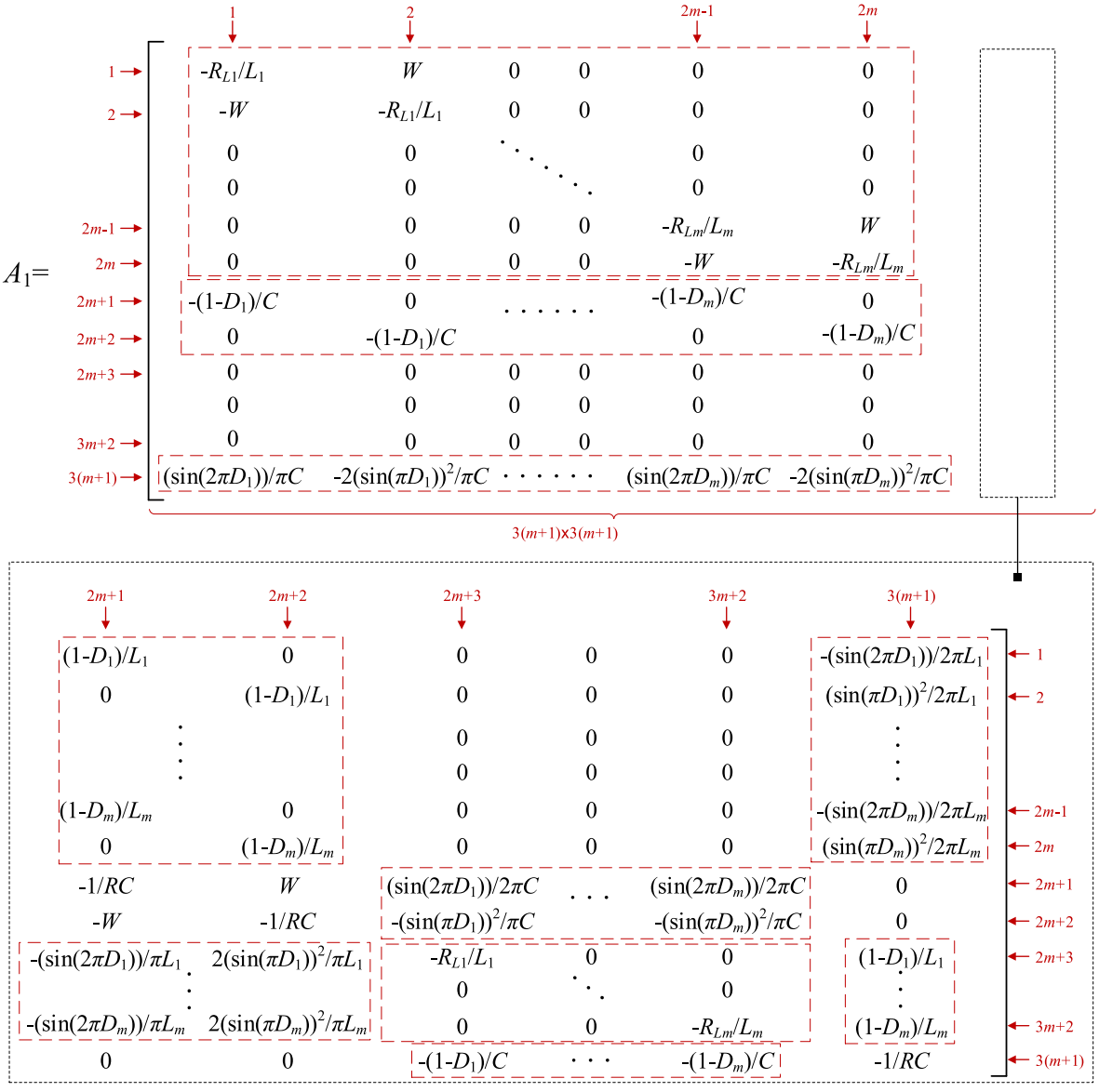
$-R_{L1}/L_1$
W
$-R_{Lm}/L_m$
$-W$
$-(1-D_1)/C$
$-(1-D_m)/C$
$(\sin(2\pi D_1))/\pi C$
$-2(\sin(\pi D_1))^2/\pi C$
$(\sin(2\pi D_m))/\pi C$
$-2(\sin(\pi D_m))^2/\pi C$
$3(m+1)$x$3(m+1)$
$(1-D_1)/L_1$
$(1-D_m)/L_m$
$-1/RC$
$-(\sin(2\pi D_1))/2\pi L_1$
$(\sin(\pi D_1))^2/2\pi L_1$
$-(\sin(2\pi D_m))/2\pi L_m$
$(\sin(\pi D_m))^2/2\pi L_m$
$(\sin(2\pi D_1))/2\pi C$
$-(\sin(\pi D_1))^2/\pi C$
$(\sin(2\pi D_m))/2\pi C$
$-(\sin(\pi D_m))^2/\pi C$
$-(\sin(2\pi D_1))/\pi L_1$
$2(\sin(\pi D_1))^2/\pi L_1$
$-(\sin(2\pi D_m))/\pi L_m$
$2(\sin(\pi D_m))^2/\pi L_m$

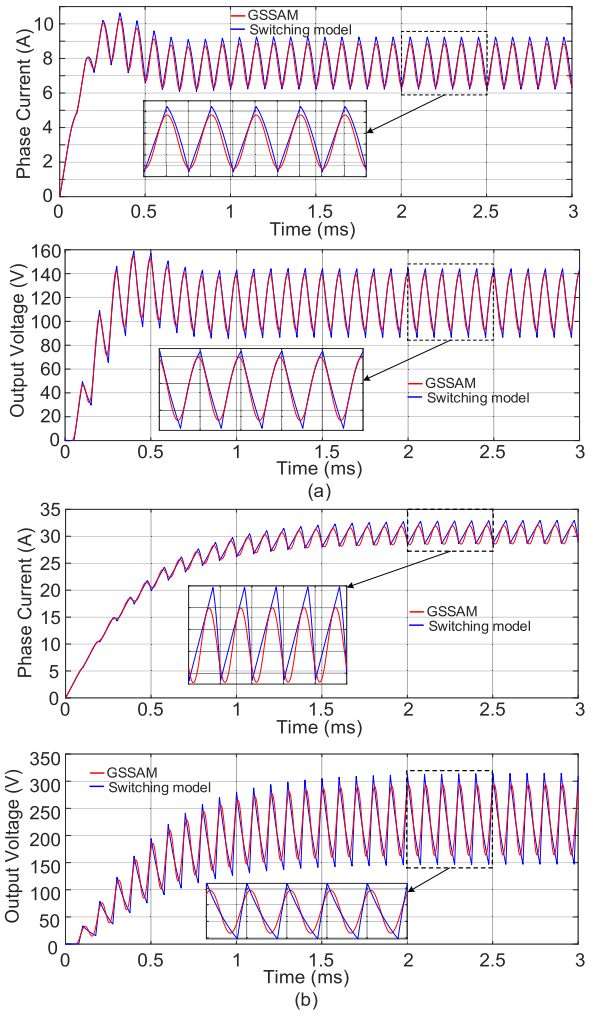

FIGURE 5. Boost converter dynamics from the switching model and GSSAM at duty cycle equals to (a) 0.5. (b) 0.75.

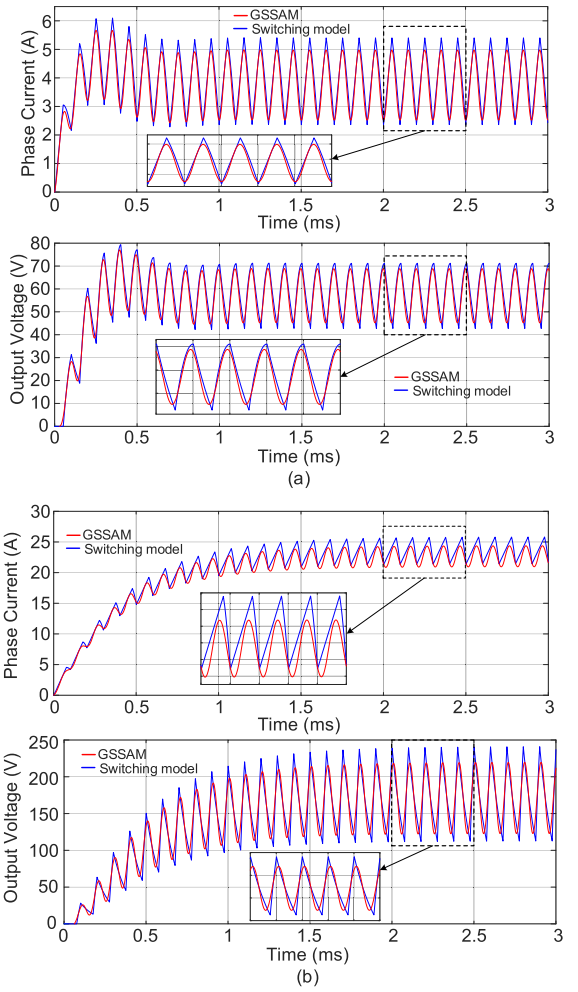

FIGURE 6. Buck-boost converter dynamics from the switching model and GSSAM at duty cycle equals to (a) 0.5. (b) 0.75.

the error from the GSSAM of buck converter is lower than the error of the boost and the buck-boost converters. In [8], the complexity of the converter is represented by how far is the state-space matrix from the Jordan form square matrix, so that the closer is the converter state space matrix to the Jordan form square matrix, the less complex the converter will be.

3) SWITCHING FREQUENCY

The switching frequency is another factor that affects the error between the GSSAM and the switching model which is not shown in the simulation results. When the switching frequency is much higher than the converter natural frequency which depends on the RLC load, the first order approximation is enough to represent the converter oscillatory behavior as the RLC combination acts like a low pass filter and filters higher order harmonics. While in the case of switching frequency is less than the natural frequency, higher order harmonics will exist in the system so that the first order approximation is not enough. As a result, the proper design of converters should have a switching frequency higher than the converter natural frequency to prevent the existence of high order harmonics [8], [9].

B. PHASE SWITCHING DYNAMICS

The number of operating phases in multi-phase converters is directly proportional to the output load power, so that the maximum efficiency condition is always maintained over the entire operating range. Therefore, it is important to test the GSSAM during switching phases on and off. The boost converter is considered for that purpose to compare the switching dynamics between the switching model and the GSSAM.

1) SWITCHING ON DYNAMICS

Fig. 7 compares steady-state and transient dynamics between the GSSAM and the switching model during switching on the second and third phases (Phase 2 and Phase 3). Fig. 7 shows that the GSSAM and the switching model have the same steady state dynamics, but the transient period is different. The difference in the transient period appears only at switching on and not at switching off as will be shown later. Hence, it can be due to the simulation solver or the PLECS model considers a non-linear effect of a stray inductance when the phase is switched on.

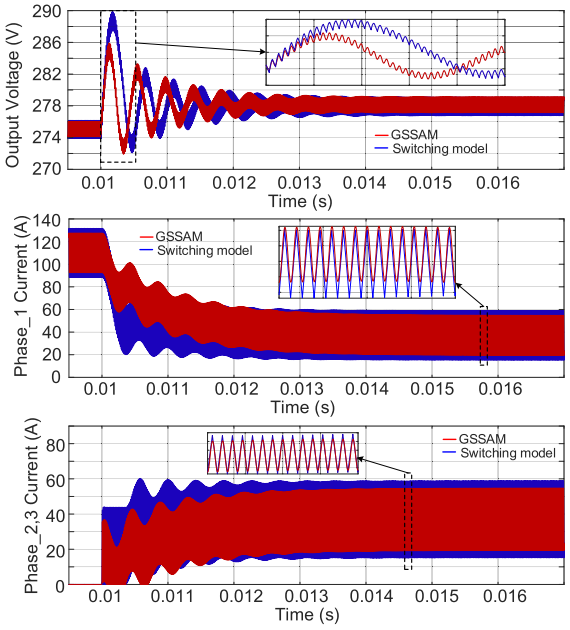

FIGURE 7. Boost converter dynamics from the switching model and GSSAM at duty cycle equals to 0.5 during switching on Phase 2 and Phase 3 when inductor parasitic inductance is considered.

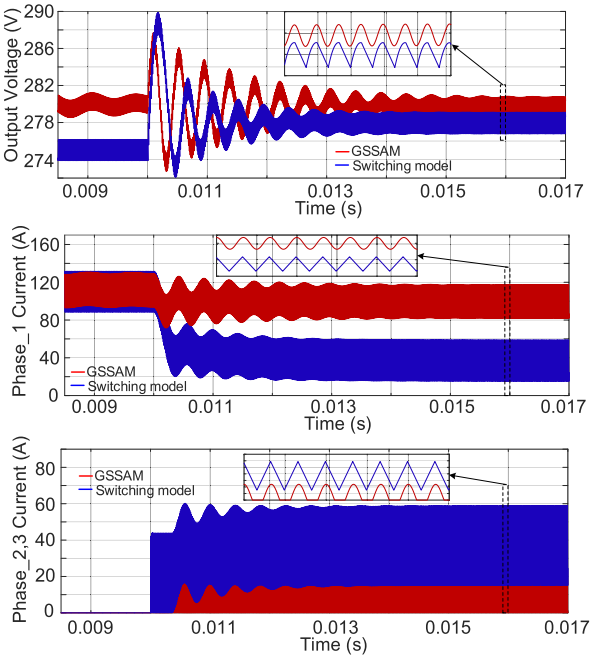

FIGURE 8. Boost converter dynamics from the switching model and GSSAM at duty cycle equals to 0.5 during switching on Phase 2 and Phase 3 when inductor parasitic resistance is ignored.

It is worth mentioning that the single phase GSSAM in [8]–[10] neglects inductor parasitic resistance for simplicity. Fig. 8 shows system dynamics during switching on Phase 2 and Phase 3 when the inductor parasitic resistance is ignored in the GSSAM. Fig. 8 shows that the zero-order harmonic of the state variables (x_9, x_{10}, x_{11} & x_{12}) does not change after switching on the two phases so that their average current is still zero. In order to understand how the inductor parasitic inductance affects the switching dynamics. Phases 2 and 3 are switched on and phase 1 is already at steady sate. Thus, the rate of change of the zero-order harmonic of Phase 1 current x_9^o in (23) is equal to zero:

$$\frac{dx_9}{dt} = \frac{\sin(2\pi D_1)}{\pi L_1} - \frac{2(\sin(\pi D_1))^2}{\pi L_1} - \frac{R_{L1}}{L_1}x_9 - \frac{-(1-D_1)}{L_1}x_{12} + \frac{V_{in}}{L_1} = 0 \tag{27}$$

$$\frac{R_{L1}}{L_1}x_9 = \frac{\sin(2\pi D_1)}{\pi L_1} - \frac{2(\sin(\pi D_1))^2}{\pi L_1} - \frac{-(1-D_1)}{L_1}x_{12} + \frac{V_{in}}{L_1} \tag{28}$$

The second phase is switched on by controlling its duty cycle to be equal to Phase 1 duty cycle to ensure equal current sharing, thus,

$$D_2 = D_1 \tag{29}$$

$$\frac{dx_{10}}{dt} = \frac{x_{10,k+1} - x_{10,k}}{T_s} = \frac{\sin(2\pi D_2)}{\pi L_2} - \frac{2(\sin(\pi D_2))^2}{\pi L_2} - \frac{R_{L2}}{L_2}x_{10,k} - \frac{-(1-D_2)}{L_2}x_{12} + \frac{V_{in}}{L_2}(30) \tag{30}$$

'$x_{10,k}$' is Phase 2 current at the instant of switching, which is equal to zero, therefore (30) with the help of (29) can be modified to:

$$\frac{x_{10,k+1}}{T_s} = \frac{\sin(2\pi D_1)}{\pi L_2} - \frac{2(\sin(\pi D_1))^2}{\pi L_2} - \frac{-(1-D_1)}{L_2}x_{12} + \frac{V_{in}}{L_1} \tag{31}$$

Substituting (28) in (31):

$$\frac{x_{10,k+1}}{T_s} = \frac{R_{L1}}{L_1}x_9 \tag{32}$$

Equation (32) shows the value of Phase 2 current after switching on Phase 2. It can be concluded that by neglecting the inductor parasitic resistance, the zero-order harmonic of Phase 2 current keeps zero after switching since R_{L1} is zero. Similarly, ignoring inductor resistance also affects switching off.

2) SWITCHING OFF DYNAMICS

If the converter operation is changed from 3-phase to 2-phase at time instant t_k, Phase 3 current must decay to zero at the next time instant t_{k+1}. Thus, the state variables of the zero order and the first order harmonic of the switched phase current i_{Li} are equal to zero at the instant t_{k+1}:

$$x_{2i-1}^o = \frac{x_{2i-1,k+1} - x_{2i-1,k}}{T_s} = \frac{-x_{2i-1,k}}{T_s} \tag{33}$$

$$x_{2i}^o = \frac{x_{2i,k+1} - x_{2i,k}}{T_s} = \frac{-x_{2i,k}}{T_s} \tag{34}$$

$$x_{2(m+1)+i}^o = \frac{x_{2(m+1)+i,k+1} - x_{2(m+1)+i,k}}{T_s} = \frac{-x_{2(m+1)+i,k}}{T_s} \tag{35}$$

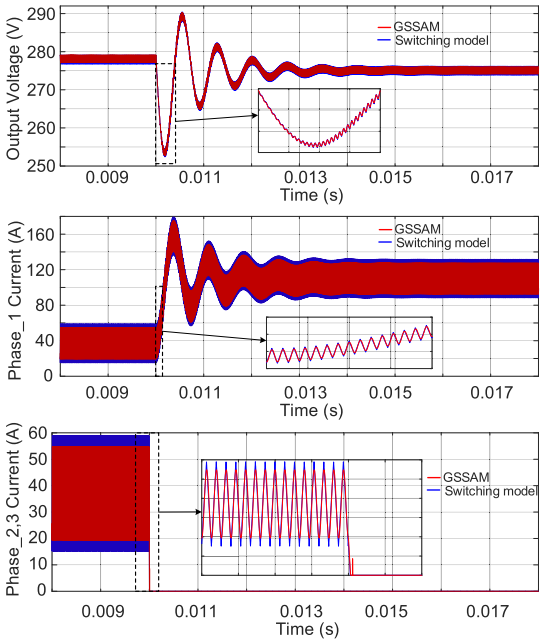

FIGURE 9. Boost converter dynamics from the switching model and GSSAM at duty cycle equals to 0.5 during switching off phase 2 and phase 3.

As mentioned before x_{2i-1} and x_{2i} are the state variables of the first order harmonic of i_{Li} and $x_{2(m+1)+i}$ is the state variable of the zero order harmonic of i_{Li}. Equations (33)-(35) describe the state variables of the phase or phases which are switched off. Fig. 9 shows the converter dynamics when Phase 2 and Phase 3 are switched off and it reveals that the GSSAM can describe the converter dynamics during switching phases off after considering (33)-(35).

IV. CONCLUSION

The generalized state space average models (GSSAMs) for multi-phase buck, boost and buck-boost DC-DC converters are investigated. The GSSAM has the advantage of describing the oscillatory behavior which is dominant in resonant converters and high ripples DC-DC converters, where the AC signals in system dynamics cannot be neglected. System dynamics in GSSAM is represented by the zero and the first order harmonics of Fourier series. The proposed model of the three converters is compared and validated with PLECS switching model. Multi-phase interleaved DC-DC converters are used to achieve the maximum efficiency over the entire operating range, so that the number of operating phases increases with the required output power. Thus, transient and steady-state dynamics during switching phases on and off are included in the GSSAM. Simulation results showed that when the inductor parasitic resistance is ignored, the GSSAM or even the conventional average model cannot represent switching dynamics.

REFERENCES

[1] M. Kankam and M. Elbuluk, "A survey of power electronics applications in aerospace technologies," in *Proc. 36th Intersoc. Energy Convers. Eng. Conf.* Savannah, GA, USA: ASME, IEEE, AICHE, ANS, SAE, and AIAA, 2001, pp. 147–153.

[2] K. Emadi and M. Ehsani, "Aircraft power systems: Technology, state of the art, and future trends," *IEEE Aerosp. Electron. Syst. Mag.*, vol. 15, no. 1, pp. 28–32, Jan. 2000.

[3] R. Karimi, D. Kaczorowski, A. Zlotnik, and A. Mertens, "Loss optimizing control of a multiphase interleaving DC-DC converter for use in a hybrid electric vehicle drivetrain," in *Proc. IEEE Energy Convers. Congr. Expo. (ECCE)*, Milwaukee, WI, USA, Sep. 2016, pp. 1–8.

[4] T. Schoenen, M. S. Kunter, M. D. Hennen, and R. W. De Doncker, "Advantages of a variable DC-link voltage by using a DC-DC converter in hybrid-electric vehicles," in *Proc. IEEE Vehicle Power Propuls. Conf.*, Lille, France, Sep. 2010, pp. 1–5.

[5] K. J. Karimi, A. Booker, and A. Mong, "Modeling, simulation, and verification of large DC power electronics systems," in *Proc. PESC Record. 27th Annu. IEEE Power Electron. Spec. Conf.*, Baveno, Italy, Jun. 1996, pp. 1731–1737.

[6] P. Azer, R. Rodriguez, J. Guo, J. Gareau, J. Bauman, H. Ge, B. Bilgin, and A. Emadi, "Time-efficient integrated electrothermal model for a 60-kW three-phase bidirectional synchronous DC–DC converter," *IEEE Trans. Ind. Appl.*, vol. 56, no. 1, pp. 654–668, Jan. 2020.

[7] P. Azer, R. Rodriguez, H. Ge, J. Bauman, P. S. Ravi, and A. Emadi, "Time efficient integrated electro-thermal model for bidirectional synchronous DC-DC converter in hybrid electric vehicles," in *Proc. IEEE Transp. Electrific. Conf. Expo (ITEC)*, Long Beach, CA, USA, Jun. 2018, pp. 55–62.

[8] A. Emadi and A. Abur, "Real time state estimation of multi-converter DC power electronic systems using generalized state space averaging method," in *Proc. IEEE 33rd Annu. IEEE Power Electron. Spec. Conf.*, Denver, CO, USA, Jun. 2002, pp. 1001–1007.

[9] J. Mahdavi, A. Emaadi, M. D. Bellar, and M. Ehsani, "Analysis of power electronic converters using the generalized state-space averaging approach," *IEEE Trans. Circuits Syst. I, Fundam. Theory Appl.*, vol. 44, no. 8, pp. 767–770, Aug. 1997.

[10] V. A. Caliskan, O. C. Verghese, and A. M. Stankovic, "Multifrequency averaging of DC/DC converters," *IEEE Trans. Power Electron.*, vol. 14, no. 1, pp. 124–133, Jan. 1999.

[11] M. M. Jalla, A. Emadi, G. A. Williamson, and B. Fahimi, "Modeling of multi-converter more electric ship power systems using the generalized state space averaging method," in *Proc. 30th Annu. Conf. IEEE Ind. Electron. Soc. (IECON)*, Nov. 2004, pp. 508–513.

[12] S. R. Sanders, J. M. Noworolski, X. Z. Liu, and G. C. Verghese, "Generalized averaging method for power conversion circuits," *IEEE Trans. Power Electron.*, vol. 6, no. 2, pp. 251–259, Apr. 1991.

[13] A. W. Green, "Modelling a push-pull parallel resonant convertor using generalised state-space averaging," *IEE Proc. B Electr. Power Appl.*, vol. 140, no. 6, pp. 350–356, 1993.

[14] A. Nasiri and A. Emadi, "Modeling, simulation, and analysis of active filter systems using generalized state space averaging method," in *Proc. IECON-29th Annu. Conf. IEEE Ind. Electron. Soc.*, Nov. 2003, pp. 1999–2004.

[15] Z. Lin and H. Ma, "Modeling and analysis of three-phase inverter based on generalized state space averaging method," in *Proc. IECON-39th Annu. Conf. IEEE Ind. Electron. Soc.*, Vienna, Austria, Nov. 2013, pp. 1007–1012.

[16] A. Yazdani and R. Iravani, "A generalized state-space averaged model of the three-level NPC converter for systematic DC-voltage-balancer and current-controller design," *IEEE Trans. Power Del.*, vol. 20, no. 2, pp. 1105–1114, Apr. 2005.

[17] K. Corzine, X. Kou, and J. R. Baker, "Dynamic average-value modeling of a four-level drive system," *IEEE Trans. Power Electron.*, vol. 18, no. 2, pp. 619–627, Mar. 2003.

[18] A. Emadi, "Modelling of power electronic loads in AC distribution systems using the generalized state space averaging method," in *Proc. IECON-27th Annu. Conf. IEEE Ind. Electron. Soc.*, Denver, CO, USA, Nov./Dec. 2001, pp. 1008–1014.

[19] C. Gaviria, R. Grino, and E. Fossas, "Control scheme based on GSSA modeling applied to an unity power factor boost rectifier," in *Proc. IEEE Conf. Control Appl. (CCA)*, vol. 1, Jun. 2003, pp. 582–587.

[20] C. Gaviria, E. Fossas, and R. Grino, "Robust controller for a full-bridge rectifier using the IDA approach and GSSA modeling," *IEEE Trans. Circuits Syst. I, Reg. Papers*, vol. 52, no. 3, pp. 609–616, Mar. 2005.

[21] J. Peng, B. Fan, J. Duan, Q. Yang, and W. Liu, "Adaptive decentralized output-constrained control of single-bus DC microgrids," *IEEE/CAA J. Automatica Sinica*, vol. 6, no. 2, pp. 424–432, Mar. 2019.
[22] B. Fan, J. Peng, J. Duan, Q. Yang, and W. Liu, "Distributed control of multiple-bus microgrid with paralleled distributed generators," *IEEE/CAA J. Automatica Sinica*, vol. 6, no. 3, pp. 676–684, May 2019.

PETER AZER (Graduate Student Member, IEEE) received the bachelor's and master's degrees in electrical engineering from Ain Shams University, Cairo, Egypt, in 2013 and 2016, respectively. He is currently pursuing the Ph.D. degree in electrical and computer engineering with McMaster University, Hamilton, ON, Canada. His areas of research include power electronics, motor drives, switched reluctance machines (SRM), multilevel inverters, fault-tolerant control, and system modeling.

ALI EMADI (Fellow, IEEE) received the B.S. and M.S. degrees (Hons.) in electrical engineering from the Sharif University of Technology, Tehran, Iran, in 1995 and 1997, respectively, and the Ph.D. degree in electrical engineering from Texas A&M University, College Station, TX, USA, in 2000. Before joining McMaster University, Hamilton, ON, Canada, he was the Harris Perlstein Endowed Chair Professor of engineering and the Director of the Grainger Laboratories, Electric Power and Power Electronics Center, Illinois Institute of Technology (Illinois Tech), Chicago, where he established research and teaching facilities as well as courses in power electronics, motor drives, and vehicular power systems. He was the Founder, the Chairman, and the President of Hybrid Electric Vehicle Technologies, Inc., (HEVT)—a university spin-off company of Illinois Tech. He is currently the Canada Excellence Research Chair Laureate with McMaster University. He is also the holder of the NSERC/FCA Industrial Research Chair in electrified powertrains and the Tier I Canada Research Chair in transportation electrification and smart mobility. He is the principal author/coauthor of over 450 journals and conference papers as well as several books, including *Vehicular Electric Power Systems*, in 2003, *Energy Efficient Electric Motors*, in 2004, *Uninterruptible Power Supplies and Active Filters*, in 2004, *Modern Electric, Hybrid Electric, and Fuel Cell Vehicles* (Second edition, 2009), and *Integrated Power Electronic Converters and Digital Control*, in 2009. He is also the Editor of *Handbook of Automotive Power Electronics and Motor Drives*, in 2005, and *Advanced Electric Drive Vehicles*, in 2014. He is also a Co-Editor of *Switched Reluctance Motor Drives* in 2018. He was a recipient of numerous awards and recognitions. He was the Advisor of the Formula Hybrid Teams, Illinois Tech, and McMaster University, which won the GM Best Engineered Hybrid System Award at the 2010, 2013, and 2015 competitions. He was the Inaugural General Chair of the 2012 IEEE Transportation Electrification Conference and Expo (ITEC) and has chaired several IEEE and SAE conferences in the areas of vehicle power and propulsion. He is the Founding Editor-in-Chief of the IEEE TRANSACTIONS ON TRANSPORTATION ELECTRIFICATION.